A NUMERICAL METHOD FOR LARGE-EDDY SIMULATION ON UNSTRUCTURED GRIDS

Maria Vittoria Salvetti[1], **Simone Camarri**[1], **Alain Dervieux**[3], **Bruno Koobus**[2], **Hilde Ouvrard**[2], **Stephen Wornom**[4]

[1] *Dip. Ingegneria Aerospaziale, Università di Pisa, Via G. Caruso 8, 56122 Pisa, Italy.*
[2] *Département de Mathématiques, Université de Montpellier II, Place E. Bataillon, 34095 Montpellier, France.*
[3] *INRIA, 2004 Route des Lucioles, 06902 Sophia-Antipolis, France.*
[4] *Société Lemma, 938 Avenue de la République, 06550 La Roquette-sur-Siagne, France.*

1. INTRODUCTION

The most widely used approach for the simulation of *complex* turbulent flows is the one based on the Reynolds-Averaged Navier-Stokes equations (RANS). For complex flows, we mean flows characterized by complex geometry and high Reynolds numbers, as most of the flows of industrial or engineering interest. However, RANS models usually have difficulties in providing accurate predictions for flows with massive separations or significant unsteadiness, as for instance the flow around bluff bodies. An alternative approach is the Large-Eddy simulation (LES), which, for massively separated flows, is generally more accurate, but computationally more expensive, than RANS.

The success of a large-eddy simulation depends on the combination and interaction of different factors, viz. the numerical discretization, which also provides filtering when no explicit one is applied, the grid refinement and quality, and the physical closure model. On the other hand, all these aspects can be seen as possible sources of error in LES. Up to now, most of the simulations reported in the literature are limited to moderate Reynolds numbers and simple geometries, and a few (almost generally accepted) best practices for LES have been identified in this academic context. However, these best practices are difficult to be followed in LES of complex flows and, thus, some open issues and controversial points remain before LES can be considered a completely reliable tool for industrial or engineering applications.

In particular, in this context the use of *unstructured grids* becomes particularly attractive, because of their friendliness when applied to complex realistic geometries, although they are more demanding from the point of view of computational resources. However, high-order conservative schemes, usually recommended for LES in the academic context, are expensive and difficult to be devised for unstructured grids. Although there are a few examples of numerical schemes especially developed for LES on unstructured grids (see e.g. Mahesh et al. [25]), our choice was to start from an existing numerical technology for industrial application and, in particular, from a *second-order co-located scheme*. The most critical point with co-located schemes is, in our opinion, the need of *numerical dissipation*. To better understand why, it is useful to examine how LES works.

The classical LES approach relies on the addition to the usual Navier-Stokes equations of a sub-grid scale (SGS) term and assumes that this same term is rather optimal for both turbulence modeling and numerical scheme stabilization. Similarly to Direct Numerical Simulation (DNS), it has been stated by many authors that the approximation should be of the highest possible accuracy order and preferably without any numerical dissipation. In that case, the

damping of any high frequency component is performed exclusively by the SGS terms. It is not useless to recall that in general, these terms are second-order derivatives of the flow variables (e.g. in eddy-viscosity models). Conversely, in a different approach, the role of SGS terms is completely fulfilled by a purely numerical stabilization term inside the approximation. A typical example is the MILES method [14] in which both subgrid modeling and numerical stabilization rely on monotonic dissipation by again a second order derivative (e.g. FCT (Flux-Corrected Transport) or TVD (Total-Variation Diminishing) schemes). However this family of model-free monotone methods seems to need a much larger number of nodes in the mesh for a given prediction quality.

Conversely, if monotone schemes are combined with a classical LES model, they can interact unfavorably with it, and significantly deteriorate the results (see, for instance, Garnier et al. [11]). Thus, it appears that in a reasonable option, the effects of numerical dissipation and of the SGS model should be separated as much as possible. Our proposition was to dedicate the subgrid modeling to a physics-based model and to use a second-order accurate MUSCL upwind scheme involving no TVD limiters. This co-located scheme was equipped with a tunable dissipation made of *fourth-order* [6] or *sixth-order* [5] spatial derivatives of all flow variables through a flux splitting. Fourier analysis clearly shows that such a dissipation has a damping effect which is much more localized on high frequencies than the one of stabilizations based on second-order derivatives. In this way we can reduce the interaction between, on one hand, numerical dissipation which damps in priority the highest frequencies, in particular those for which the phase error is too large and can produce oscillations, and on the other hand SGS modeling which should reproduce the effects of unresolved frequencies on the resolved ones. Moreover, a key coefficient (γ_s) permits to tune numerical dissipation to the smallest amount required to stabilize the simulation.

We also pushed forward this concept and we started to investigate the application of a locally super-convergent scheme [17], that is a scheme which is second-order accurate on the whole unstructured mesh but enjoys accuracy up to 5th order in regions where the grid is Cartesian. This is achieved by applying the linear reconstruction proposed in [5] to flux functions rather than to flow variables.

Finally, for time advancing we explored the suitability for LES of a linearized implicit scheme [26]. In particular, we investigated whether large time steps, unreachable with explicit time advancing because of stability limitations, can be employed in LES without loosing significant information on the resolved scales.

As for SGS modeling, our first choice was to use *classical* models, viz. the Smagorinsky one [37] and its dynamic version [12]. As well known, we found that the dynamic model generally gives more accurate results than the Smagorinsky one (see, e.g., Camarri et al. [6, 5]). However, due to the explicit filtering required in the dynamic procedure which is highly computationally demanding on unstructured grids, the increase in computational cost for the dynamic model was found to be rather dramatic, much larger than for structured grids or spectral schemes. On the other hand, a good compromise between accuracy and computational requirements was obtained through the Variational MultiScale approach (VMS), which was found to give the same accuracy as the dynamic model at costs comparable to those of the Smagorinsky model [16]. As will be described in the following, the main idea of VMS-LES is to decompose, through Galerkin projection, the resolved scales into the largest and smallest ones and to add the SGS model only to the smallest ones [15]. A formulation of the VMS approach for unstructured grids and the mixed finite-volume/finite-difference scheme, used in the present work, was provided by Koobus and Farhat [16].

Another major difficulty for the success of LES for the simulation of complex flows is the fact

that the cost of LES increases as the flow Reynolds number is increased. Indeed, the grid has to be fine enough to resolve a significant part of the turbulent scales, and this becomes particularly critical in the near-wall regions. Hybrid models have recently been proposed in the literature in which RANS and LES approaches are combined together in order to obtain simulations as accurate as in the LES case but at reasonable computational costs. In this context, we proposed a new strategy for blending RANS and LES approaches in a hybrid model, not described here for sake of brevity. We refer to [36, 32, 35] for details on this topic.
The paper is organized as follows: the *classical* LES approach together with the different considered closure models are briefly presented in Sec. 2. The main numerical ingredients are summarized in Sec. 3 and, in particular, the discretization of the convective terms and the linearized implicit time advancing strategy are described. The VMS-LES approach is briefly introduced in Sec. 4. Examples of academic and engineering oriented applications of the set-up methodology are then presented in Sec. 5. Conclusions are finally drawn in Sec. 6.

2. CLASSICAL LES APPROACH AND SGS MODELS

The LES approach consists in filtering in space the Navier-Stokes equations, in order to get rid of the high frequency fluctuations, and in simulating directly only the filtered flow. Due to the non-linearity of the problem, the filtered equations contain some unknown terms which represent the effect of the eliminated fluctuations on the filtered flow. These terms need to be modeled. The filtered Navier-Stokes equations for compressible flows and in conservative form are considered. In our simulations, filtering is implicit, i.e. the numerical discretization of the equations is considered as a filter operator (grid filter).
In modeling the SGS terms resulting from filtering the Navier-Stokes equations, it is assumed that high Reynolds numbers flows are simulated, in which low compressibility effects are present in the SGS fluctuations. In addition, we assume that heat transfer and temperature gradients are moderate. Thus, the retained SGS term in the momentum equation is the classical SGS stress tensor:

$$M_{ij} \;=\; \overline{\rho u_i u_j} \;-\; \overline{\rho}\tilde{u}_i\tilde{u}_j \;\;, \tag{1}$$

where the over-line denotes the grid filter and the tilde the density-weighted Favre filter ($\tilde{f} = \left(\overline{\rho f}\right) / \left(\overline{\rho}\right)$). The isotropic part of M_{ij} can be neglected under the assumption of low compressibility effects in the SGS fluctuations [8]. The deviatoric part, T_{ij}, is expressed by an eddy viscosity term:

$$T_{ij} = -2\mu_{\text{sgs}}\left(\widetilde{S_{ij}} - \frac{1}{3}\widetilde{S_{kk}}\right) \;\;, \tag{2}$$

$\widetilde{S_{ij}}$ being the resolved strain tensor, μ_{sgs} the SGS viscosity.
In the total energy equation, the effect of the SGS fluctuations has been modeled by the introduction of a constant SGS Prandtl number to be *a priori* assigned:

$$Pr_{\text{sgs}} = C_p\frac{\mu_{\text{sgs}}}{K_{\text{sgs}}} \tag{3}$$

where K_{sgs} is the SGS conductivity coefficient; it takes into account the diffusion of total energy caused by the SGS fluctuations and is added to the molecular conductivity coefficient. We refer to Camarri and Salvetti [3] and Camarri et al. [6] for a more detailed discussion of the simplifying assumptions leading to the adopted SGS modeling.
The different eddy-viscosity models used in the present work are briefly recalled in the following.

2.1 Smagorinsky model

In the Smagorinsky model the eddy viscosity is defined as follows:

$$\mu_{\mathrm{s}} = \overline{\rho} \left(C_{\mathrm{s}}\Delta\right)^2 \left|\widetilde{S}\right| \quad , \tag{4}$$

where Δ is the filter width and C_{s} is a constant that must be *a priori* assigned and $\left|\widetilde{S}\right| = \sqrt{2\widetilde{S_{ij}}\widetilde{S_{ij}}}$ (repeated indexes imply summation). To complete the definition of the SGS viscosity, the grid filter width must be specified. Since filtering is implicitly applied by the numerical discretization, there is no unique rigorous definition of the filter width. The following expression has been employed here for each grid element j:

$$\Delta^{(j)} = Vol_j^{1/3} \tag{5}$$

where Vol_j is the volume of the $j-th$ grid element.

2.2 Dynamic model

The dynamic version of the Smagorinsky model has also been considered. The dynamic procedure proposed by Germano [12] is applied to the compressible Smagorinsky model described in the previous section. In this way, the coefficient that must be *a priori* assigned in the Smagorinsky model (C_{s}) is computed as a function of space at each time step. We have chosen to dynamically compute $(C_{\mathrm{s}}\Delta)^2$ instead of C_{s}^2, as in the classical dynamic model, in order to avoid the indetermination in the definition of the filter width. The test filter used here consists in P1-averaging the flow variables on all the elements having a given node as a vertex. The ratio $\widehat{\Delta}/\Delta$ ($\widehat{\Delta}$ being the test filter width), which is the only quantity to be *a priori* assigned in the dynamic model, is defined on each node as: $\widehat{\Delta}/\Delta = \sqrt[3]{N}$, where N is the number of elements having the node as a vertex. This is a consequence of the assumption that the size of the implicit filter scales as the cubic root of the element volume. A local smoothing is applied to avoid unphysical oscillations of $(C_{\mathrm{s}}\Delta)^2$. For more details on the implementation of this model see Camarri and Salvetti [3].

2.3 Vreman model

The eddy viscosity μ_v of the Vreman model [43] is defined by:

$$\mu_v = \overline{\rho} C_V \left(\frac{B_\beta}{\alpha_{ij}\alpha_{ij}}\right)^{\frac{1}{2}} \tag{6}$$

with

$$\alpha_{ij} = \partial\tilde{u}_j/\partial x_i$$

$$\beta_{ij} = \Delta^2 \alpha_{mi}\alpha_{mj}$$

$$B_\beta = \beta_{11}\beta_{22} - \beta_{12}^2 + \beta_{11}\beta_{33} - \beta_{13}^2 + \beta_{22}\beta_{33} - \beta_{23}^2$$

The constant is set to $C_V \approx 2.5C_s^2$ where C_s denotes the Smagorinsky constant. The filter width Δ has been defined as done for the Smagorinsky model.

2.4 WALE model

The last considered SGS closure is the Wall-Adapting Local Eddy -Viscosity (WALE) SGS model proposed by Nicoud and Ducros [27]. The eddy-viscosity term μ_w of the model is defined by:

$$\mu_W = \overline{\rho}(C_W\Delta)^2 \frac{(\widetilde{S_{ij}}^d \widetilde{S_{ij}}^d)^{\frac{3}{2}}}{(\widetilde{S_{ij}}\widetilde{S_{ij}})^{\frac{5}{2}} + (\widetilde{S_{ij}}^d \widetilde{S_{ij}}^d)^{\frac{5}{4}}} \tag{7}$$

with

$$\widetilde{S_{ij}}^d = \frac{1}{2}({g_{ij}}^2 + {g_{ji}}^2) - \frac{1}{3}\delta_{ij}{g_{kk}}^2$$

being the symmetric part of the tensor ${g_{ij}}^2 = g_{ik}g_{kj}$, where $g_{ij} = \partial\tilde{u}_i/\partial x_j$. The constant C_W is set to 0.1.

3. NUMERICAL METHOD

The LES governing equations are discretized in space using a mixed finite-volume/finite-element method applied to unstructured tetrahedrizations. The adopted scheme is vertex centered, i.e. all degrees of freedom are located at the vertexes. P1 Galerkin finite elements are used to discretize the diffusive terms.

3.1 Convective fluxes

A dual finite-volume grid is obtained by building a cell C_i around each vertex i; two different ways of constructing the finite-volume cells are considered. Cells of the first type (*median cells*, MC) are built by the rule of medians: the boundaries between cells are made of triangular interface facets. Each of these facets has a mid-edge, a facet centroid, and a tetrahedron centroid as vertexes. The second type of cells (*new generation cells*, NGC) can be obtained in 3D as follows: to build the cell centered at node i, let us consider all the neighboring nodes of i (j). For each element containing the nodes i and j, the cell surface is given by the triangles connecting the middle of the edge joining these two vertexes, the *surface center* of the faces of the element having this edge in common, and the *volume center* of the element. The *surface center* of a given face is the center of its circumscribed circle, if the face comprises only acute angles, otherwise it is the middle of its longest edge, and the *volume center* of an element is the center of its circumscribed sphere if the former is located inside the element, otherwise, it is the surface center (among those of the four tetrahedron faces), which is closest to the center of the circumscribed sphere. Although the NGC, as well as the MC, can be built starting from a generic tetrahedrization, it is interesting to consider the case of a Cartesian mesh, thus, made of rectangle parallelepipeds (thereafter called *bricks*), which are cut in a particular way in tetrahedrons, following [13]. This division splits each brick in six identical tetrahedrons, each being the mirror image of its neighbors (see Fig. 1(a)). Starting from such a tetrahedization, the NGC cells are bricks, centered around the vertexes of the mesh, as can be seen in Fig. 1b, in which the trace of the division of an element into NGC is shown.
The convective fluxes are discretized on this tessellation by a finite-volume approach, i.e. in terms of the fluxes through the common boundaries between each couple of neighboring cells:

$$\sum_{j\in V(i)} \int_{\partial C_{ij}} \mathcal{F}\left(W, \vec{n}\right) d\sigma \quad , \tag{8}$$

where $V(i)$ is the set of neighboring nodes to vertex i, ∂C_{ij} is the boundary between cells C_i and C_j, and $\vec{n}$ is the outer normal to the cell C_i and $\mathcal{F}\left(W, \vec{n}\right)$ the Euler flux in the direction of $\vec{n}$.

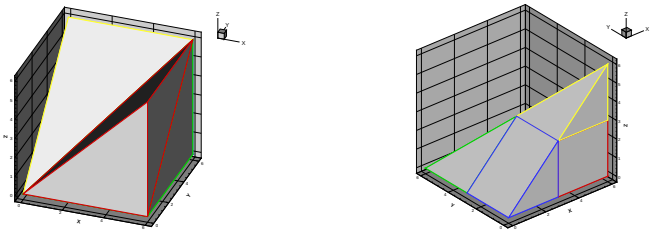

(a) (b)

Figure 1: New finite-volume cells in 3D: (a) division in tetrahedrons, (b) trace of NGC on a tetrahedron resulting from the previous division.

In all the schemes considered herein, the unknowns are discontinuous along the cell boundaries and this allows an approximate Riemann solver to be introduced.

3.1.1 Second-order accurate scheme providing numerical dissipation proportional to high-order space derivatives

The Roe scheme [34] (with Turkel preconditioning) represents the basic upwind component for the numerical evaluation of the convective fluxes $\mathcal{F}$:

$$\int_{\partial C_{ij}} \mathcal{F}\left(W, \vec{n}\right) d\sigma \simeq \Phi^R\left(W_i,\ W_j,\ \vec{n}\right) = \frac{\mathcal{F}\left(W_i,\ \vec{n}\right) + \mathcal{F}\left(W_j,\ \vec{n}\right)}{2} - \gamma_s d^R\left(W_i,\ W_j,\ \vec{n}\right) \quad (9)$$

$$d^R\left(W_i,\ W_j,\ \vec{n}\right) = P^{-1}|P\mathcal{R}\left(W_i,\ W_j,\ \vec{n}\right)| \frac{W_j - W_i}{2} \quad (10)$$

in which W_i is the unknown vector at the i-th node, $\vec{n}$ is the normal to the cell boundary and $\mathcal{R}$ is the Roe Matrix. The matrix $P(W_i,\ W_j)$ is the Turkel-type preconditioning term, introduced to avoid accuracy problems at low Mach numbers [41]. Finally, the parameter γ_s multiplies the upwind part of the scheme and permits a direct control of the numerical viscosity, leading to a full upwind scheme (the usual Roe scheme) for $\gamma_s = 1$ and to a centered scheme when $\gamma_s = 0$.

The spatial accuracy of this scheme is only first order. The MUSCL linear reconstruction method ("Monotone Upwind Schemes for Conservation Laws"), introduced by Van Leer [42], is employed to increase the order of accuracy of the Roe scheme. The basic idea is to express the Roe flux as a function of a reconstructed value of W at the boundary between the two cells centered respectively at nodes i and j: $\Phi^R\left(W_{ij},\ W_{ji},\ \vec{n}_{ij}\right)$. W_{ij} and W_{ji} are extrapolated from the values of W at the nodes, as follows:

$$W_{ij} = W_i + \frac{1}{2}\left(\vec{\nabla}W\right)_{ij} \cdot \vec{ij} \quad (11)$$

$$W_{ji} = W_j - \frac{1}{2}\left(\vec{\nabla}W\right)_{ji} \cdot \vec{ij} \quad (12)$$

Schemes with different properties can be obtained by different numerical evaluation of the *slopes* $\left(\vec{\nabla}W\right)_{ij}.\vec{ij}$ and $\left(\vec{\nabla}W\right)_{ji}.\vec{ij}$. All the considered reconstructions can be written in the following general form:

$$\begin{aligned}(\vec{\nabla}W)_{ij}.\vec{ij} = \ & (1-\beta)(\vec{\nabla}W)^C_{ij}.\vec{ij} + \beta(\vec{\nabla}W)^U_{ij}.\vec{ij} \\ & +\xi_c\left[(\vec{\nabla}W)^U_{ij}.\vec{ij} - 2(\vec{\nabla}W)^C_{ij}.\vec{ij} + (\vec{\nabla}W)^D_{ij}.\vec{ij}\right] \\ & +\xi_d\left[(\vec{\nabla}W)_M.\vec{ij} - 2(\vec{\nabla}W)_i.\vec{ij} + (\vec{\nabla}W)_j.\vec{ij}\right]\end{aligned} \quad (13)$$

With reference to Fig. 2, $(\vec{\nabla}W)_{ij}^{U}$ is the gradient on the upwind tetrahedron T_{ij}, $(\vec{\nabla}W)_{ij}^{D}$ is the gradient on the downwind tetrahedron T_{ji}, $(\vec{\nabla}W)_i$ is the nodal gradient computed over the finite-volume cell around node i, $(\vec{\nabla}W)_j$ is the nodal gradient computed over the finite-volume cell around node j, $(\vec{\nabla}W)_{ij}^{C}$ is the centered gradient ($(\vec{\nabla}W)_{ij}^{C}.\vec{ij} = W_j - W_i$) and $(\vec{\nabla}W)_M$ is the gradient at the point M. This last gradient is computed by interpolation of the nodal gradient values at the nodes contained in the face opposite to i in the upwind tetrahedron T_{ij}. The reconstruction of W_{ji} is analogous.

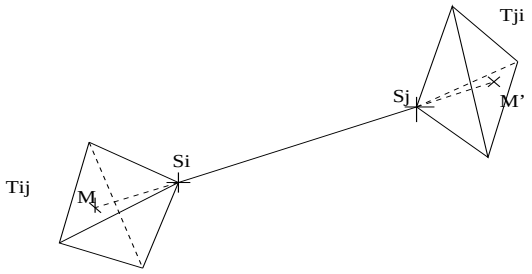

Figure 2: Sketch of points and elements involved in the computation of gradients.

In choosing a particular set of free coefficients (β, ξ_c, ξ_d) in Eq. (13) attention has been dedicated to the dissipative properties of the resulting scheme which is a key point for its successful use in LES simulations. Two schemes have been proposed: the first on (V4) [6] is characterized by $\beta = 1/3$, $\xi_c = \xi_d = 0$, while the latter (V6) [5] is obtained by $\beta = \frac{1}{3}$, $\xi_c = -\frac{1}{30}$ and $\xi_d = -\frac{2}{15}$.

The numerical dissipation in the schemes V4 and V6 is made of fourth- and sixth-order space derivatives, respectively, and, thus, it is concentrated on a narrow-band of the highest resolved frequencies. This is important in LES simulations to limit as far as possible the interactions between numerical and SGS dissipation, which could deteriorate the accuracy of the results.

3.1.2 Super-convergent scheme

The same kind of reconstruction as in the previous section is applied to the fluxes, instead of to the flow variables. Thus, the following numerical flux is obtained:

$$\Phi_{ij} = \frac{\mathcal{F}_{ij} + \mathcal{F}_{ji}}{2} - \frac{1}{2}\,\gamma_s P^{-1} sign(P\mathcal{R})P\,(\mathcal{F}_{ji} - \mathcal{F}_{ij})$$

where $\mathcal{F}_{ij}$ and $\mathcal{F}_{ji}$ are the extrapolated fluxes at the cell interface, computed through the V6 reconstruction scheme. Let A be a generic matrix such that $A = T^{-1}\Lambda(A)T$, T being the matrix of the eigenvectors of A and $\Lambda(A) = diag(\lambda_i(A))$ the diagonal matrix whose elements are the eigenvalues of A, the notation $sign(A)$ means $T^{-1}diag(sign(\lambda_i(A)))T$. The resulting numerical approximation of the convective fluxes (V6NL) is 5th-order accurate for a conformal tetrahedrization obtained from a Cartesian grid as described previously. Indeed, by interpolating the fluxes, the second-order limitation for MUSCL reconstruction can be overcome. More details on this super-convergent scheme can be found in [17].

3.2 Time advancing

Simulations can be advanced in time both with explicit or implicit schemes. In the first case, low-storage Runge-Kutta schemes are used.

As for the implicit time advancing, a second-order time-accurate backward difference scheme is adopted:

$$\frac{3W^{n+1} - 4W^n + W^{n-1}}{2\Delta t} + \psi^{n+1} = 0 \tag{14}$$

in which ψ^{n+1} denotes the discretized convective fluxes, diffusive and SGS terms evaluated at time step $n+1$.

To avoid the solution of a non linear system at each time step, the scheme (14) can be linearized by using the Jacobian of ψ^{n+1} with respect to the unknown variables. However, the evaluation of the Jacobian of ψ^{n+1} for the second-order accurate spatial discretization previously described and the solution of the resulting linear system implies significant computational costs and memory requirements. Thus, a defect-correction technique [26] is used here, which consists in iteratively solving simpler problems obtained through an approximate linearization of (14). Thus, the following approximation is introduced:

$$\psi^{n+1} \simeq \psi^n + J_1^n (W^{n+1} - W^n)$$

in which J_1^n is the exact Jacobian of the spatial discretization terms when the convective fluxes are evaluated at first order. Then, the defect-correction iterations write as:

$$\begin{cases} \mathcal{W}^0 = W^n \\ \\ \left(\frac{3}{2\Delta t} Vol + J_1^s\right)(\mathcal{W}^{s+1} - \mathcal{W}^s) = -\dfrac{3\mathcal{W}^s - 4W^n + W^{n-1}}{2\Delta t} - \psi^s \qquad \text{for } s = 0, \cdots, M-1 \\ \\ W^{n+1} = \mathcal{W}^M \end{cases}$$

where Vol is the diagonal matrix containing the cell volumes and M is typically equal to 2. Indeed, it can be shown [26] that only 2 defect-correction iterations are needed to reach a second-order accuracy.

4. VARIATIONAL MULTISCALE LES

In the Variational MultiScale approach for Large Eddy Simulation (VMS-LES) the flow variables are decomposed as follows:

$$W = \underbrace{\overline{W}}_{LRS} + \underbrace{W'}_{SRS} + W^{SGS} \tag{15}$$

where $\overline{W}$ are the large resolved scales (LRS), W' are the small resolved scales (SRS) and W^{SGS} are the unresolved scales. This decomposition is obtained by projection in the LRS and SRS spaces respectively. In the present study, we follow the VMS approach proposed by Koobus and Farhat [16] for the simulation of compressible turbulent flows through a finite volume/finite element discretization on unstructured tetrahedral grids. Let ψ_l be the finite-volume basis functions and ϕ_l the N finite-element basis functions associated to the used grid. In order to obtain the VMS flow decomposition, these can be expressed as: $\psi_l = \overline{\psi}_l + \psi'_l$ and $\phi_l = \overline{\phi}_l + \phi'_l$, in which the overbar denotes the basis functions spanning the finite dimensional spaces of the large resolved scales and the prime those spanning the SRS spaces. As in [16], the basis functions of the LRS space are defined through a projector operator in the LRS space, based on spatial average on macro cells:

$$\overline{\psi}_k = \frac{Vol(C_k)}{\sum_{j \epsilon I_k} Vol(C_j)} \sum_{j \epsilon I_k} \psi_j \tag{16}$$

for finite volumes, and:

$$\overline{\phi}_k = \frac{Vol(C_k)}{\sum_{j \epsilon I_k} Vol(C_j)} \sum_{j \epsilon I_k} \phi_j \tag{17}$$

for finite elements. In both Eqs. (16) and (17), $I_k = \{j / C_j \in C_{m(k)}\}$, $C_{m(k)}$ being the macro-cell containing the cell C_k. The macro-cells are obtained by a process known as agglomeration [19]. The basis functions for the SRS space are clearly obtained as follows: $\psi'_l = \psi_l - \overline{\psi}_l$ and $\phi'_l = \phi_l - \overline{\phi}_l$.
Finally, a key feature of the VMS-LES approach is that the SGS model is added only to the smallest resolved scales. Thus, let τ_{LES} be the closure term given by one of the SGS models described in Sec. 1, it is computed as a function of the smallest resolved scales, i.e.$\tau_{LES}(W')$. Since eddy-viscosity models are used here (see Sec. 1), the SGS terms are discretized analogously to the viscous fluxes. Thus, the Galerkin projection of the corresponding term in the governing equations is given by: $(\tau_{LES}(W'), \phi'_l)$, where $(\cdot, \cdot)$ denotes the L^2 scalar product.
More details about this VMS-LES methodology can be found in Koobus and Farhat [16], Farhat et al. [9] and Ouvrard et al. [31].

5. EXAMPLES OF APPLICATIONS

Among the different applications of the set-up numerical methodology, some representative results are presented for three different type of flow configurations. The first one is the flow around a a square cylinder of infinite length, at a Reynolds number, based on the cylinder side length and on the freestream velocity, equal to 22000. This is a rather classical benchmark for LES [33] and allows the different proposed numerical and modeling ingredients to be validated through comparison with experimental data and LES results in the literature. The second test-case is the flow around a circular cylinder at very low Reynolds number (Re=3900), for which very detailed LES results and experimental data are available. It is used here to investigate the behavior of VMS-LES vs. classical LES and the effect of SGS modeling in both these approaches. Finally, the results obtained in LES and VMS-LES simulations of a more complex configuration of engineering interest are briefly summarized.

5.1 Flow past a square cylinder

As previously stated, the flow around a square cylinder of infinite length is considered, at a Reynolds number, based on the cylinder side length and on the freestream velocity, equal to 22000. A Cartesian frame of reference is considered, with the origin at the gravity center of the square section and the x and z axes oriented in the streamwise and spanwise directions, respectively. The computational domain dimensions are: $L_i/D = 5$, $L_o/D = 10$, $L_s/D = 4$ and $H/D = 7$, where D is the side length of the square section, L_i and L_o are the distances between the origin of the reference frame and the inflow and outflow boundaries, respectively, L_s is the width of the domain in the spanwise direction and H is the distance between the cylinder axis and the domain boundaries in the y direction. Boundary conditions based on Steger-Warming decomposition [40] are used at the inflow and at the outflow surfaces. On the side surfaces free-slip is imposed and the flow is assumed to be periodic in the spanwise direction. Approximate boundary conditions based on the Reichardt wall-law are used on the cylinder surface (see Camarri et al. [6] and Camarri and Salvetti [4]).
The results shown in the following have been obtained on two grids: the first (GR1) of about 10^5 nodes and 6×10^5 elements, the second (GR2), more refined, having approximately 2×10^5

LES and experiments	C_l'	$\overline{C_d}$	C_d'	l_r
S_V4_G05_GR1	0.79	1.84	0.10	1.45
S_V6_G05_GR1	0.84	1.89	0.09	1.41
S_V6_G05_GR2	1.10	2.2	0.18	1.15
D_V4_G05_GR1	0.91	2.03	0.12	1.24
D_V6_G05_GR1	0.94	2.06	0.10	1.33
D_V4_G10_GR1	0.84	1.94	0.09	1.53
D_V6_G10_GR1	0.86	2.02	0.09	1.47
D_V6_G05_GR2	1.09	2.10	0.15	1.15
V_V6_G20_GR2	1.08	2.10	0.18	1.4
S_V6NL_G20_GR3	1.17	2.33	–	1.29
Rodi et al. [33]	[0.38,1.79]	[1.66,2.77]	[0.10,0.27]	[0.89,2.96]
Sohankar et al. [38] and Fureby et al. [10]	[1.23,1.54]	[2.0,2.32]	[0.16,0.20]	[1.29-1.34]
Lyn et al. [23, 24]	-	2.1	-	1.4
Bearman et al. [1]	1.2	2.28	-	-
Norberg [29]	-	2.16	-	-
Luo et al. [22]	1.21	2.21	0.18	-

Table 1: Bulk coefficients; comparison with experimental data and with other simulations in the literature. $\overline{C_d}$ is the mean drag coefficient, C_d' and C_l' are the r.m.s. of the drag and lift coefficients and l_r is the length of the mean recirculation bubble. The name of the simulations is composed in this way: the first part indicates the turbulence model ("S" stands for the Smagorinsky model, "D" for the Dynamic one and "V" for the VMS-LES with the Smagorinsky closure), the second indicates the scheme adopted for the convective fluxes, the third indicates the value of the parameter γ_s (in hundredth), the fourth indicates the adopted grid.

nodes and 1.1×10^6 elements. The average distance of the first layer of nodes from the cylinder surface is $6 \times 10^{-2}D$ for GR1 and $4.5 \times 10^{-2}D$ for GR2. For both grids, approximately 32 nodes are located in the spanwise direction within the wake region. A third structured grid (GR3) has been considered to carry out preliminary simulations with the super-convergent scheme described in Sec. 3.1.2 (V6NL). GR3 has about 4.1×10^5 nodes and the distance of the first node from the wall is 6×10^{-3}; note also that the stretching of the elements of GR3 is significant, the maximum aspect ratio being equal to 12, while the grids GR1 and GR2 are rather homogeneous.

The main bulk coefficients obtained in the LES simulations, with the Smagorinsky model, the dynamic model and in the VMS-LES simulations with the Smagorinsky closure, are presented in Tab. 1, together with results from other LES simulations [10, 33, 38] and experimental data [1, 22, 23, 24, 29]. As shown in Tab. 1, the results obtained with the V4 scheme are sensitive to the choice of the parameter γ_s and, when this is tuned close to the minimum value compatible with numerical stability, the LES simulations gives rather accurate predictions. Nevertheless, as shown in Camarri et al. [6], the numerical viscosity gives a contribution to the fluxes which is more important than the one given by the dynamic model, while the LES model contribution is dominant when the more dissipative Smagorinsky model is used. This drawback, as well as the need of a fine tuning of the parameter γ_s have been overcome with the V6 scheme. Indeed, the results in Tab. 1 show a reduced sensitivity of the predicted bulk coefficients to γ_s when V6 is used. Moreover, the accuracy of the results is improved, especially concerning the unsteady part of the flow field. Indeed, the values of the r.m.s. of the force coefficients is generally higher

with V6 (see Tab.1). Moreover, independently of the SGS model, in the simulations with V6 a larger energy content than with V4 is found in all the resolved frequencies, and especially in the highest ones. This is well shown, for instance, in Fig. 3 where the Fourier energy spectra of the velocity signals measured in a point in the wake in D_V4_G05_GR1 and D_V6_G05_GR1 are compared. The mean convection velocity in the considered points within the wake is large enough to justify the Taylor hypothesis of frozen turbulence which allows us to assume that high time frequencies correspond to small scale in space; thus, one might conclude that small scales are less damped by the V6 scheme. As regards the SGS modeling interaction with the

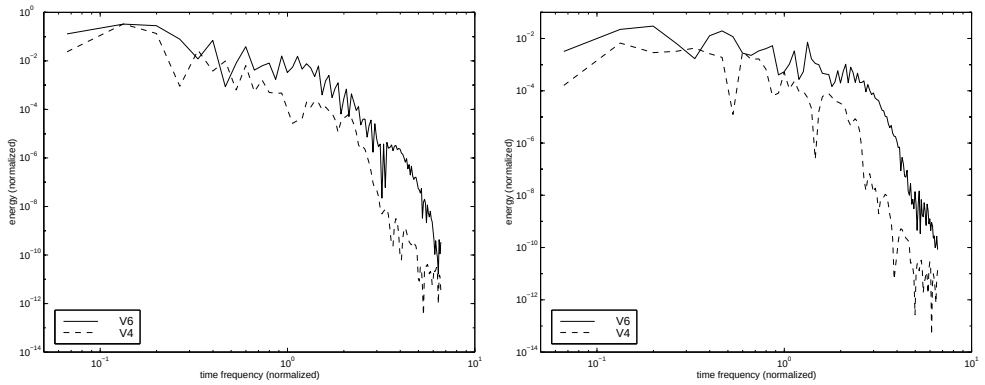

(a) (b)

Figure 3: Simulations D_V4_G05_GR1 and D_V6_G05_GR1. Fourier energy spectra of the velocity components recorded at $x = 3$, $y = 0.5$ and $z = 0$. a) Transverse velocity v; b) spanwise velocity w.

adopted numerical scheme, Tab. 1 shows that the qualitative variations of the bulk coefficients with the SGS model are the same for V4 and V6, i.e. the dynamic model generally improves predictions with respect to the Smagorinsky model. However, quantitatively, the sensitivity to SGS modeling of the results obtained with V6 is lower than with V4. This is particularly evident from the comparison of the Reynolds stresses, not shown here for the sake of brevity, and this is related to the larger energy content at the small scales obtained with V6; see Camarri et al. [5] for a more detailed discussion.

The grid refinement improves results particularly when the Smagorinsky model is used, while the simulations with the dynamic model give acceptable results also on the grid GR1. However the dynamic model is definitely more CPU-demanding than the Smagorinsky one, due to the explicit filtering required in the dynamic procedure, which is highly computationally demanding on unstructured grids. As an example, when the dynamic model is used instead of the Smagorinsky one with the V4 scheme and an explicit time advancing, an increase of about 180% CPU time per time step is measured.

The best compromise between accuracy and computational costs has been obtained by the adoption of the VMS-LES model, properly formulated for our numerics. Indeed, Tab. 1 shows that the level of accuracy of the VMS-LES model, with the Smagorinsky SGS closure, is comparable with that of the dynamic model. At the same time, its computational cost is only slightly larger than that of the Smagorinsky model. Finally, note that the problems of numerical stability typically encountered with the dynamic model, unless ad-hoc smoothing or clipping of the model coefficient values is carried out, are obviously not present in the VMS approach. A more detailed discussion of the results obtained with the VMS-LES model can be found in Ref. [16].

An example of the results obtained through the super-convergent V6NL scheme on a structured grid (GR3) is also shown in Tab. 1. A significant improvement is observed in the prediction of

Simulation	Turbulence model	SGS	aggl. level.	γ	CFL
CircCyl1	LES	Smagorinsky	-	0.3	20
CircCyl2	LES	Vreman	-	0.3	20
CircCyl3	LES	WALE	-	0.3	20
CircCyl4	VMS-LES	Smagorinsky	1	0.3	20
CircCyl5	VMS-LES	Vreman	1	0.3	20
CircCyl6	VMS-LES	WALE	1	0.3	20
CircCyl7	no model	-	-	0.3	20

Table 2: Overview of the considered simulations.

the r.m.s. of the lift coefficient, while for the other parameters the agreement with the experimental data is the same as or even worse than the one obtained with the V6 and V4 schemes. However, a more systematic validation should be carried out and, probably, the V6NL scheme for the convective fluxes should also be coupled with a more accurate discretization of the diffusive and SGS terms and tested within the VMS-LES approach.

5.2 Flow past a circular cylinder

In this section, the flow over a circular cylinder at Mach number $M_\infty = 0.1$ and Reynolds number (based on the cylinder diameter and on the freestream velocity) equal to 3900 is simulated through the VMS-LES and the traditional LES approach. The computational domain is such that $-10 \leq x/D \leq 25$, $-20 \leq y/D \leq 20$ and $-\pi/2 \leq z/D \leq \pi/2$, where x, y and z denote the streamwise, transverse and spanwise directions respectively. The cylinder of unit diameter is centered on the axis $x = y = 0$. For the purpose of these simulations, the Steger-Warming conditions [40] are imposed at the inflow and outflow as well as on the upper and lower surface ($y = \pm 20$). In the spanwise direction periodic boundary conditions are applied and on the cylinder surface no-slip boundary conditions are set.
The flow domain is discretized by an unstructured tetrahedral grid which consists of approximately 2.9×10^5 nodes. The averaged distance of the nearest point to the cylinder boundary is $0.017D$, which corresponds to $y^+ \approx 3.31$.
A large number of simulations were carried out by varying different parameters, as, for instance, the SGS model, the value of γ_s, the cell agglomeration level for VMS-LES. We report here only the results obtained in some of these simulations, in order to investigate the differences between classical LES and VMS-LES and the effect of the SGS modeling. The main parameters of the considered simulations are summarized in Tab. 2. All the simulations were carried out with the V6 scheme and the linearized implicit time advancing. In particular, the advantage of the use of an implicit clearly appears from Tab. 2, since a CFL equal to 20 could be used in all the simulations, without loosing significant information about the dynamics of the resolved scales. Indeed, it was checked that up to this value of CFL the results are independent of the adopted time step. Incidentally, the adopted CFL definition is such that the stability limit of the RK1 scheme corresponds to CFL=1.
The flow bulk parameters obtained in these simulations are reported in Tab. 3 and compared with LES results in the literature and experimental data. The averaged data are obtained over about 27 shedding cycles or 150 non-dimensional time units after the initial transient period. The effect of the SGS model is larger in the classical LES simulations (compare CircCyl1, CircCyl2 and CircCyl3) than in the VMS-LES approach (CircCyl4, CircCyl5, CircCyl6). The overall agreement with the numerical and the experimental data in the literature is better for the VMS-LES simulations than for the LES ones, especially for the mean drag coefficient, the

data from	$\overline{C_d}$	St	l_r	θ_{sep}	$\overline{C_{P_b}}$	U_{min}
CircCyl1	1.16	0.212	0.81	88	-1.17	-0.26
CircCyl2	1.04	0.221	0.97	89	-1.01	-0.28
CircCyl3	1.14	0.214	0.75	91	-1.20	-0.25
CircCyl4	1.00	0.221	1.05	88	-0.96	-0.29
CircCyl5	0.99	0.221	1.12	88	-0.91	-0.30
CircCyl6	0.96	0.225	1.24	88	-0.90	-0.30
CircCyl7	0.96	0.223	1.24		-0.88	-0.30
Numerical data						
[18]	1.04	0.210	1.35		-0.94	-0.37
[2]	1.07		1.197	87.7	-1.011	
[20]	0.99	0.212	1.36		-0.94	-0.33
Experiments						
[28]	0.99$\pm$0.05	0.215$\pm$0.05			-0.88$\pm$0.05	-0.24$\pm$0.1
[39]				86 $\pm$2		
[7]		0.215$\pm$0.005	1.33$\pm$0.05			
[30]		0.21$\pm$0.005	1.4$\pm$0.1			-0.24$\pm$0.1
[21]			1.18$\pm$0.05			

Table 3: Bulk coefficients: comparison with experimental data and with other simulations in the literature. $\overline{C_d}$ denotes the mean drag coefficient, St the Strouhal number, l_r the mean recirculation length: the distance on the centerline direction from the surface of the cylinder to the point where the time-averaged streamwise velocity is zero, θ_{sep} the separation angle, $\overline{C_{P_b}}$ the mean back-pressure coefficient and U_{min} the minimum centerline streamwise velocity.

base pressure and the mean recirculation bubble length. Finally, the results obtained without any SGS model (CircCyl7) are similar to those of the VMS-LES simulations. This could be considered as an a posteriori confirmation that the V6 scheme actually adds a viscosity which is limited to the smallest resolved scales, in the spirit of VMS-LES.
A more detailed analysis of the reliability of the results and of the different sources of error in LES and VMS-LES will be the object of forthcoming papers.

5.3 Vortex induced motion of a complex geometry

The prediction of vortex-induced motion of a complex spar geometry is an important motivation for VMS modeling. The spar geometry consists of a cylinder equipped with helical strakes, see Fig. 4. Each strake produces in the flow a shear layer that interacts with the large flow structures and inhibits to a significant extent the von Karman vortex street. We investigate the impact of the choice of a VMS model on the quality of a LES prediction. In our computations, the obstacle is maintained by elastic moorings and moves under the effect of the vortex shedding. The flow-structure coupling is computed at several reduced velocity between 4 and 9 (m/s) and Reynolds numbers between 2×10^5 and 4×10^5. The grid involves 5×10^5 vertexes. The V6 scheme and the linearized implicit time advancing have been used for these simulations.
The behavior of the transverse position of the spar is a key output to be accurately predicted. Fig. 5 shows the time variation of the transverse position of the spar at a reduced velocity of 7 m/s. The r.m.s. computed in LES with the Smagorinsky model is 0.048, and the r.m.s. in VMS-LES is 0.070, which compares better with the experimental data of 0.077. The agreement of the VMS calculations with experiments for the different velocities is demonstrated in Tab. 4.

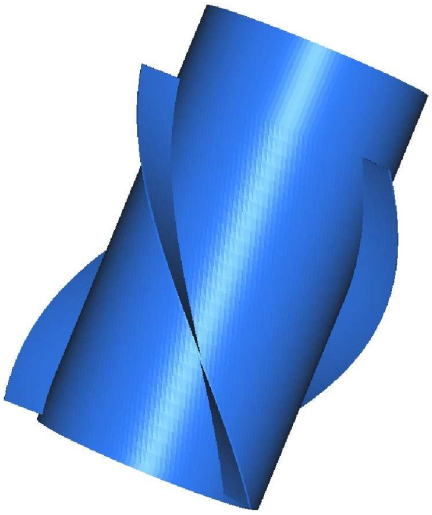

Figure 4: Spar geometry.

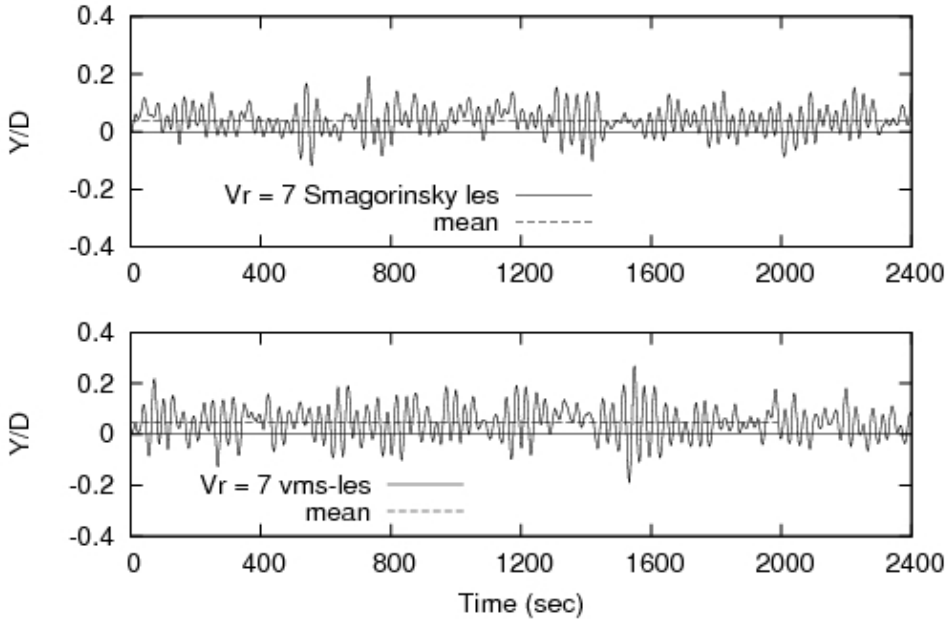

Figure 5: Time variation of the transverse position of the spar at a reduced velocity of 7 m/s.

Reduced velocity	4	5	6	7	8	9
LES	-	-	-	.048	-	-
VMS-LES	.0018	.020	.04	.070	.12	.118
Experiments	.0018	.025	.05	.077	.13	.125

Table 4: Vortex-induced motion of a spar: r.m.s. of transverse deviation

6. CONCLUDING REMARKS

The main choices made and the solutions proposed for the mutual adaption between an *industrial* numerical method, designed and validated for RANS simulations, and an LES approach to turbulence have been briefly presented in this paper. The numerical method is based on a co-located mixed finite-volume/finite-element discretization on unstructured tetrahedral grids. Diffusive fluxes are discretized by P1 finite elements and convective fluxes by finite volumes, through the Roe scheme and MUSCL reconstruction to obtain second-order accuracy in space. The key feature of our approach is a particular MUSCL reconstruction scheme, such that the introduced numerical viscosity is proportional to high-order space derivatives, viz. fourth-order derivatives (V4) or sixth-order derivatives (V6). A first step towards the set-up of super-convergent schemes for the discretization of the convective fluxes has also been briefly described. These schemes should be second-order accurate on unstructured grids and enjoy up to fifth-order accuracy on Cartesian grids. Finally, time advancing can be explicit or implicit, through a linearized defect-correction approach. As for turbulence modeling, either the classical LES approach or the VMS-LES one are used, together with different eddy-viscosity SGS models.
Examples of academic and engineering oriented applications of the set-up methodology have been given. Summarizing, the results validate our strategy of introducing a numerical viscosity proportional to high-order derivatives in space, in order to keep its effects on the smallest resolved scales and to reduce negative interactions with the SGS model. Indeed, the results obtained with the V6 scheme are in general more accurate than those obtained with the V4 scheme, also without a fine tuning of the parameter γ_s, which controls the amount of introduced numerical viscosity. It has also been shown that the use of an implicit scheme is convenient also for LES. Indeed, large time steps, unreachable with explicit time advancing because of stability limitations, can be used without loosing significant information on the dynamics of the resolved scales. Finally, the VMS-LES approach closed with a *cheap* eddy-viscosity SGS model, as for instance the Smagorinsky one, appears to be more accurate than classical LES (closed with the same type of SGS modeling), without introducing significant additional computational costs.

References

[1] P. W. Bearman and E. D. Obasaju. An experimental study of pressure fluctuations on fixed and oscillating square-section cylinders. *J. Fluid Mech.*, 119:297–321, 1982.

[2] M. Breuer. Numerical and modeling on large eddy simulation for theflow past a circular cylinder. *International Journal of Heat and Fluid Flow*, 19:512–521, 1998.

[3] S. Camarri and M. V. Salvetti. Towards the large-eddy simulation of complex engineering flows with unstructured grids. Technical Report RR-3844, INRIA, 1999.

[4] S. Camarri and M. V. Salvetti. On the approximate treatment of wall boundary conditions in large-eddy simulation. Technical Report ADIA 2002-3, Dep. Aerospace Engineering - University of Pisa, December 2002.

[5] S. Camarri, M. V. Salvetti, B. Koobus, and A. Dervieux. A low diffusion MUSCL scheme for LES on unstructured grids. *Computers and Fluids*, 33:1101–1129, 2004.

[6] S. Camarri, M.V. Salvetti, B. Koobus, and A. Dervieux. Large-eddy simulation of a bluff-body flow on unstructured grids. *Int. J. Num. Meth. Fluids*, 40:1431–1460, 2002.

[7] G.S. Cardell. *Flow past a circular cylinder with a permeable splitter plate*. PhD thesis, Graduate Aeronautical Lab., California Inst. of Technology, 1993.

[8] G. Erlebacher, M. Y. Hussaini, C. G. Speziale, and T. A. Zang. Toward the large-eddy simulation of compressible flows. *J. Fluid Mech.*, 238:155–185, 1992.

[9] C. Farhat, A. Kajasekharan, and B. Koobus. A dynamic variational multiscale method for large eddy simulations on unstructured meshes. *Computational Methods in Applied Mechanics and Engineering*, pages 1688–1691, 2005.

[10] C. Fureby, G. Tabor, H. G. Weller, and A. D. Gosman. Large eddy simulation of the flow around a square prism. *AIAA Journal*, 38(3):442–452, 2000.

[11] E. Garnier, P. Sagaut, P. Comte, and M. Deville. On the use of shock-capturing schemes for large-eddy simulation. *J. Comp. Phys*, 153:273–311, 1999.

[12] M. Germano, U. Piomelli, P. Moin, and W. Cabot. A dynamic subgrid-scale eddy viscosity model. *Phys. Fluids A*, 3(7):1760–1765, 1991.

[13] N. Gourvitch, G. Rogé, I. Abalakin, A. A: Dervieux, and T. Kobuzskaya. A tetrahedral-based superconvergent scheme for aeroacoustics. Technical Report RR-5215, INRIA, 2004.

[14] F.F. Grinstein and C. Fureby. From canonical to complex flows: Recent progress on monotonically integrated les. *Computing in Science and Engineering*, 6(2):36–49, 2006.

[15] T.J.R. Hughes, L. Mazzei, and K.E. Jansen. Large eddy simulation and the variational multiscale method. *Comput. Vis. Sci.*, 3:47–59, 2000.

[16] B. Koobus and C. Farhat. A variational multiscale method for the large eddy simulation of compressible turbulent flows on unstructured meshes-application to vortex shedding. *Comput. Methods Appl. Mech. Eng.*, 193:1367–1383, 2004.

[17] B. Koobus, S. Wornom, S. Camarri, M.V. Salvetti, and A. Dervieux. Nonlinear V6 schemes for compressible flows. Technical Report RR-6433, INRIA, 2008.

[18] A.G. Kravchenko and P. Moin. Numerical studies of flow over a circular cylinder at re=3900. *Physics of fluids*, 12(2):403–417, 1999.

[19] M.H. Lallemand, H. Steve, and A. Dervieux. Unstructured multigridding by volume agglomeration: current status. *Comput. Fluids*, 21:397–433, 1992.

[20] J. Lee, N. Park, S. Lee, and H. Choi. A dynamical subgrid-scale eddy viscosity model with a global model coefficient. *Physics of Fluids*, 18(12), 2006.

[21] L.M. Lourenco and C. Shih. Characteristics of the plane turbulent near weak of a circular cylinder. a particle image velocimetry study, (data taken from kravchenko and moin).

[22] S. C. Luo, MdG. Yazdani, Y. T. Chew, and T. S. Lee. Effects of incidence and afterbody shape on flow past bluff cylinders. *J. Ind. Aerodyn.*, 53:375–399, 1994.

[23] D. A. Lyn, S. Einav, W. Rodi, and J. H. Park. A laser-doppler velocimeter study of ensemble-averaged characteristics of the turbulent near wake of a square cylinder. *J. Fluid Mech.*, 304:285–319, 1995.

[24] D.A. Lyn and W. Rodi. The flapping shear layer formed by flow separation from the forward corner of a square cylinder. *J. Fluid Mech.*, 267:353–376, 1994.

[25] K. Mahesh, G. Constantinescu, and P. Moin. A numerical method for large-eddy simulation in complex geometries. *J. Comp. Phys.*, 197(1):215–240, 2004.

[26] R. Martin and H. Guillard. A second-order defect correction scheme for unsteady problems. *Comput. and Fluids*, 25(1):9–27, 1996.

[27] F. Nicoud and F. Ducros. Subgrid-scale stress modelling based on the square of the velocity gradient tensor. *Flow Turbulence and Combustion*, 62(3):183–200, 1999.

[28] C. Norberg. Effects of reynolds number and low-intensity free-sream turbulence on the flow around a circular cylinder. *Publ. No. 87/2, Department of Applied Termosc. and Fluid Mech., Chalmer University of Technology, Gothenburg, Sweden*, 1987.

[29] C. Norberg. Flow around rectangular cylinders: pressure forces and wake frequencies. *J. Wind Eng. Ind. Aerodyn.*, 49:187–196, 1993.

[30] L. Ong and J. Wallace. The velocity field of the turbulent very near wake of a circular cylinder. *Exp. in Fluids*, 20:441–453, 1996.

[31] H. Ouvrard, S. Wornom, B. Koobus, M.V. Salvetti, S. Camarri, and A. Dervieux. Computation of complex unsteady flows around bluff bodies through VMS-LES modeling. In *Proceedings of West-East High Speed Flow Field Conference*, November 2007.

[32] G. Pagano, S. Camarri, M.V. Salvetti, B. Koobus, and A. Dervieux. Strategies for RANS/VMS-LES coupling. Technical Report RR-5954, INRIA, 2006.

[33] W. Rodi, J. H. Ferziger, M. Breuer, and M. Pourquié. Status of large eddy simulation: results of a workshop. *ASME J. Fluids Eng.*, 119:248–262, 1997.

[34] P.L. Roe. Approximate Riemann solvers, parameters, vectors and difference schemes. *J. Comp. Phys.*, 43:357–372, 1981.

[35] M.V. Salvetti, S. Camarri, B.Koobus, and A. Dervieux. LES and hybrid RANS/LES simulation of complex flows on unstructured grids. In *Proceedings of the West-East high speed flow field conference*. CD, 2007.

[36] M.V. Salvetti, B. Koobus, S. Camarri, and A. Dervieux. Simulation of bluff-body flows through a hybrid RANS/VMS-LES model. In *Proceedings of the IUTAM Symposium on Unsteady Separated Flows and their Control*, Corfu (Grece), June 18-22 2007.

[37] J. Smagorinsky. General circulation experiments with the primitive equations. *Monthly Weather Review*, 91(3):99–164, 1963.

[38] A. Sohankar, L. Davidson, and C. Norberg. Large eddy simulation of flow past a square cylinder: comparison of different subgrid scale models. *ASME J. Fluids Eng.*, 122:39–47, 2000.

[39] J. Son and T.J. Hanratty. Velocity gradient of the wall for flow around a circular cylinder at reynolds numbers from 5000 to 100000. *J. Fluid Mech.*, 35:353–368, 1969.

[40] J.L. Steger and R.F. Warming. Flux vector splitting for the inviscid gas dynamic equations with applications to the finite difference methods. *J. Comp. Phys*, 40(2):263–293, 1981.

[41] E. Turkel. Review of preconditioning methods of fluid dynamics. *Appl. Num. Math.*, 12:257–284, 1993.

[42] B. van Leer. Towards the ultimate conservative scheme. IV: A new approach to numerical convection. *J. Comp. Phys.*, 23:276–299, 1977.

[43] A.W. Vreman. An eddy-viscosity subgrid-scale model for turbulent shear flow: algebraic theory and application. *Physics of Fluids*, 16:3670–3681, 2004.